Article

Cell Reports

Paxillin-Mediated Recruitment of Calcineurin to the Contractile Ring Is Required for the Correct Progression of Cytokinesis in Fission Yeast

Graphical Abstract

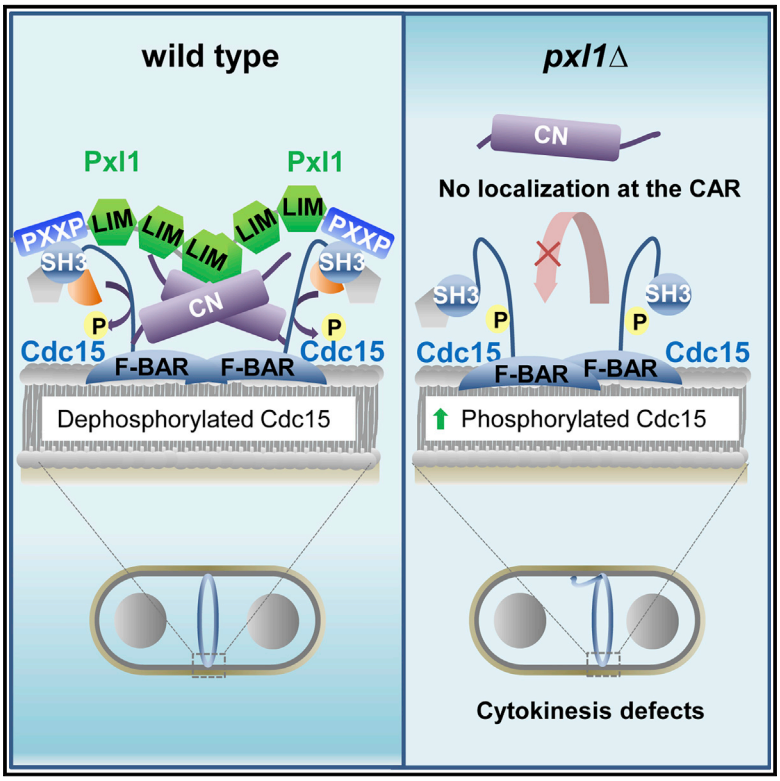

Highlights

- Pxl1 recruits calcineurin (CN) phosphatase to the cell division site
- CN collaborates with Bgs1 in septum ingression
- CN increases the concentration of Pxl1 and other Cdc15 binding partners
- CN dephosphorylates Cdc15 both *in vivo* and *in vitro*

Authors

Rebeca Martín-García, Victor Arribas, Pedro M. Coll, ..., Jaime Correa-Bordes, Juan Carlos Ribas, Pilar Pérez

Correspondence

piper@usal.es

In Brief

Martín-García et al. show that fission yeast paxillin binds and recruits calcineurin (CN) phosphatase to the cytokinetic actomyosin ring (CAR). There, CN collaborates with Bgs1 in septum ingression and promotes the concentration of Pxl1 at the CAR in a feedback loop likely mediated through CN dephosphorylation of the Cdc15 F-BAR protein, essential for cytokinesis.

Martín-García et al., 2018, Cell Reports *25*, 772–783
October 16, 2018
https://doi.org/10.1016/j.celrep.2018.09.062

CellPress

OPEN ACCESS
CellPress

Cell Reports
Article

Paxillin-Mediated Recruitment of Calcineurin to the Contractile Ring Is Required for the Correct Progression of Cytokinesis in Fission Yeast

Rebeca Martín-García,[1,5] Victor Arribas,[1,5] Pedro M. Coll,[1,5] Mario Pinar,[2] Raul A. Viana,[1] Sergio A. Rincón,[3] Jaime Correa-Bordes,[4] Juan Carlos Ribas,[1] and Pilar Pérez[1,6,*]

[1]Instituto de Biología Funcional y Genómica, Consejo Superior de Investigaciones Científicas (CSIC) and Departamento de Microbiología y Genética, Universidad de Salamanca, Salamanca, Spain
[2]Departamento de Biología Celular y Molecular, Centro de Investigaciones Biológicas del CSIC, Madrid 28040, Spain
[3]Institut Curie, PSL Research University, CNRS, UMR 144, 75005 Paris, France
[4]Departamento de Ciencias Biomédicas, Universidad de Extremadura, Badajoz, Spain
[5]These authors contributed equally
[6]Lead Contact
*Correspondence: piper@usal.es
https://doi.org/10.1016/j.celrep.2018.09.062

SUMMARY

Paxillin is a scaffold protein that participates in focal adhesion signaling in mammalian cells. Fission yeast paxillin ortholog, Pxl1, is required for contractile actomyosin ring (CAR) integrity and collaborates with the β-glucan synthase Bgs1 in septum formation. We show here that Pxl1's main function is to recruit calcineurin (CN) phosphatase to the actomyosin ring; and thus the absence of either Pxl1 or calcineurin causes similar cytokinesis defects. In turn, CN participates in the dephosphorylation of the Cdc15 F-BAR protein, which recruits and concentrates Pxl1 at the CAR. Our findings suggest the existence of a positive feedback loop between Pxl1 and CN and establish that Pxl1 is a crucial component of the CN signaling pathway during cytokinesis.

INTRODUCTION

Calcineurin (CN) is a type 2B phosphatase dependent on Ca^{2+}/calmodulin that is highly conserved from yeast to human (Cyert, 2001). CN is a heterodimer composed of a catalytic subunit (CN A) that includes a calmodulin-binding domain and an autoinhibitory domain, as well as a regulatory subunit (CN B) that binds to Ca^{2+} through four EF hands.

In mammals, CN dephosphorylates and activates transcription factors of the NFAT (nuclear factor of the activated T cell) family that promote the transcription of a wide range of genes participating in different processes, such as T cell activation, muscle heart development, apoptosis, learning and memory, neuronal plasticity, and oxidative stress (Minami, 2014). In fungi, CN regulates survival responses to environmental stresses (Juvvadi et al., 2014) and is important for pathogenic fungi virulence (Juvvadi et al., 2017). CN signaling is partially mediated by dephosphorylation and nuclear localization of conserved fungal transcription factors such as Crz1 in *Saccharomyces cerevisiae* and *Candida albicans* (Stathopoulos and Cyert, 1997; Hameed et al., 2011), Prz1 in *Schizosaccharomyces pombe* (Hirayama et al., 2003), CrzA in *Aspergillus nidulans* (Cramer et al., 2008), and SP1 in *Cryptococcus neoformans* (Adler et al., 2011). Additionally, CN signals through many targets that differ among divergent fungi (Goldman et al., 2014; Park et al., 2016).

Fission yeast *S. pombe* has a single gene encoding the CN catalytic subunit, Ppb1 (Yoshida et al., 1994), and a single gene encoding the regulatory subunit, Cnb1 (Sio et al., 2005). In this organism, CN activates at least two distinct signaling pathways, Prz1-dependent and Prz1-independent. The latter participates in the regulation of chloride homeostasis, cytokinesis, cell polarity, membrane trafficking, cell integrity, and mating (Hirayama et al., 2003; Fang et al., 2009; Kume et al., 2011; Ma et al., 2011; Cadou et al., 2013; Viana et al., 2013).

Cytokinesis is the final process of the cell cycle that produces two daughter cells. It involves the assembly of a contractile actomyosin ring (CAR) that is connected to the plasma membrane and promotes the cleavage furrow formation. In fungi, which have a cell wall, cytokinesis requires the synthesis of a division septum coordinated with the CAR constriction. Fission yeast septum forms in the cell middle and includes a primary septum containing linear β(1,3)glucan synthesized by the membrane enzyme Bgs1 (Cortés et al., 2007) and a secondary septum that forms the cell wall of the daughter cells' new ends. Loss of Bgs1 results in CAR sliding and instability, suggesting that CAR linkage to the membrane and cell wall is important for its maintenance (Arasada and Pollard, 2014).

A variety of fission yeast proteins have been implicated in the CAR anchorage to the membrane (Willet et al., 2015; Pérez et al., 2016; Rincon and Paoletti, 2016). Two major proteins with this role are Cdc15 and Imp2, which have an N-terminal Fes/CIP4 homology Bin-amphiphysin-RVS (F-BAR) domain and a C-terminal SH3 domain. The F-BAR domain allows membrane binding and oligomerization. Additionally, through its F-BAR domain, Cdc15 recruits the formin Cdc12 to promote F-actin nucleation (Carnahan and Gould, 2003).

The SH3 domain is a scaffold that binds many proteins, including the paxillin ortholog Pxl1 (Roberts-Galbraith et al.,

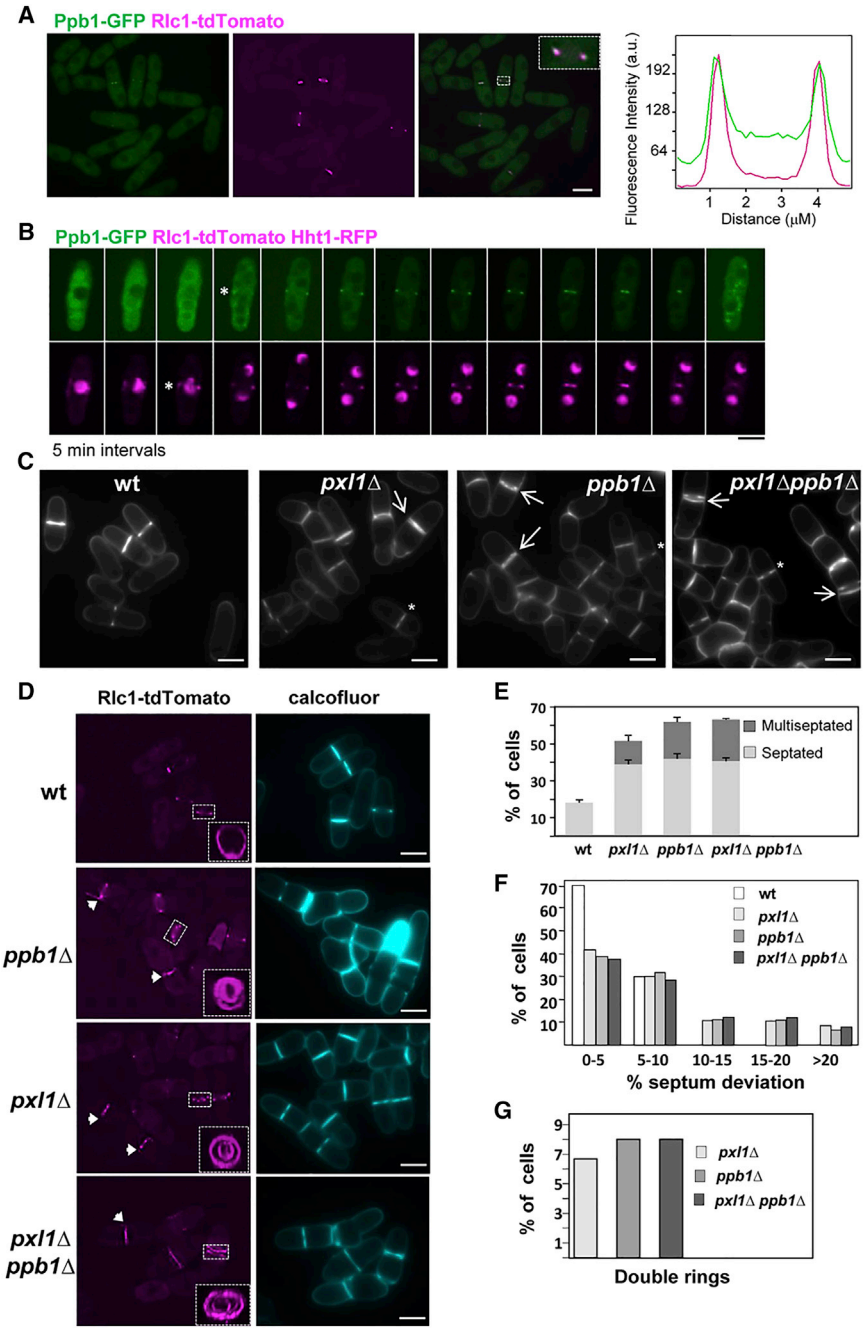

Figure 1. Calcineurin Localizes to the CAR during Cytokinesis and Is Important for CAR Contraction

(A) Fluorescence microscopy of cells with Ppb1-GFP and Rlc1-tdTomato. Right: fluorescence line scan of the region in the insert.

(B) Time-lapse images (single focal planes captured at 5 min intervals) from cells expressing Ppb1-GFP, Rlc1-tdTomato, and Hht1-RFP. Asterisks indicate the first appearance of Ppb1 or Rlc1 as a ring.

(C) Calcofluor-stained images of wild-type (wt), *pxl1*Δ, *ppb1*Δ, and *pxl1*Δ *ppb1*Δ cells. Arrows show some double septa, and asterisks indicate some off-centered septa.

(D) Micrographs of the same strains carrying Rlc1-tdTomato and stained with calcofluor. Arrows mark aberrant and double CARs. The inserts show three-dimensional maximum projection reconstructions (28 z slides at 0.3 μm intervals) from the CARs inside the white boxes.

(E–G) Quantification of the cytokinesis defects: septation and multiseptation (E), septum deviation (F), and double rings (G) observed in (C) and (D); n = 150 cells for each strain and graph; in (E) three technical replicates were made.

Scale bars, 5 μm. See also Figure S1A.

2009; Ren et al., 2015). Paxillin is a LIM domain-containing protein localized at focal adhesions in animal cells, in which it serves to adhere the plasma membrane to the extracellular matrix. In *S. pombe*, Pxl1 plays an important role in CAR anchoring and integrity (Ge and Balasubramanian, 2008; Pinar et al., 2008) and collaborates with Bgs1 in the formation of a furrow for septum progression (Cortés et al., 2015). We describe here the function of Pxl1, as a scaffold protein that enables CN function in cytokinesis by mediating its localization to the CAR. Pxl1 physically interacts with CN catalytic subunit Ppb1. Artificial localization of CN to the CAR by its fusion with the N terminus of Pxl1 is enough to suppress the cytokinesis defects caused by the absence of Pxl1 LIM domains. Our findings establish that paxillin is a crucial component of the CN signaling pathway that regulates cytokinesis.

RESULTS

CN Localizes to the CAR during Cytokinesis, and the Absence of CN Causes Cytokinesis Defects Similar to Those Caused by the Lack of Paxillin

S. pombe CN-deficient cells have defects in cell separation and some cells exhibit aberrant CARs. Additionally, they have negative genetic interactions with myosin and the septation initiation network (Yoshida et al., 1994; Zhang et al., 2000; Yada et al., 2001; Cheng et al., 2002; Fujita et al., 2002; Lu et al., 2002). To further understand the function of CN in septum formation and/or separation, we first studied its localization in a strain carrying the type II myosin regulatory chain fused to the tandem tomato protein (Rlc1-tdTomato) and the CN catalytic subunit fused to GFP (Ppb1-GFP). Ppb1-GFP localized to the cytoplasm during interphase and also concentrated to the CAR during cytokinesis (McDonald et al., 2017), co-localizing with Rlc1-tdTomato (Figure 1A). We then constructed a strain that expressed

Ppb1-GFP, Rlc1-tdTomato, and Hht1 histone fused to RFP in order to determine the time of Ppb1 arrival to the division site. Time-lapse fluorescence microscopy showed that Ppb1-GFP was recruited when the CAR was already formed and the nuclei separation was initiated but contraction had not started (Figure 1B). Ppb1-GFP remained at the ring until the end of contraction, suggesting that CN function during cytokinesis is performed from the CAR and occurs during CAR contraction and simultaneous septum synthesis.

The cytokinesis phenotypes of CN-null strains are very similar to those described in *pxl1*Δ cells (Fujita et al., 2002; Lu et al., 2002; Ge and Balasubramanian, 2008; Pinar et al., 2008), suggesting that CN and paxillin may function in the same signaling pathway. We analyzed the percentage of septated and multiseptated cells, as well as the percentage of cells with off-centered septa in cultures of wild-type, *pxl1*Δ, *ppb1*Δ (lacking the CN catalytic subunit), and *pxl1*Δ *ppb1*Δ double-mutant strains (Figures 1C–1F). We also visualized double rings formed in the same strains expressing Rlc1-tdTomato (Figures 1D and 1G). The percentages of septated, multiseptated cells, off-centered septa, and double rings were similar in *pxl1*Δ, *ppb1*Δ, and *pxl1Δ ppbΔ* double-mutant cells (Figures 1E–1G). These results indicate that the two mutations were not additive and suggest that CN and paxillin act in the same signaling pathway. Supporting this hypothesis, cells lacking Pxl1 exhibited certain phenotypes characteristic of *ppb1*Δ cells, such as hypersensitivity to $MgCl_2$, and *pxl1*Δ *ppb*Δ double-mutant cells were only slightly more sensitive (Figure S1A). Moreover, several gene mutations that are synthetically lethal with *pxl1*Δ, such as *cdc15ΔSH3*, *imp2ΔSH3*, and *fic1*Δ, were also synthetically lethal with *ppb1*Δ (Roberts-Galbraith et al., 2009; Cortés et al., 2015).

To corroborate that Pxl1 and CN were in the same signaling pathway, we checked if CN and Bgs1, the enzyme responsible for the synthesis of the primary septum, collaborated in septum formation, as Pxl1 and Bgs1 do (Cortés et al., 2015). We used a strain where *bgs1*$^+$ gene was expressed under the *nmt1-81* promoter repressible by thiamine (Cortés et al., 2015). P*nmt81-bgs1*$^+$ repression in wild-type, *pxl1*Δ, and *ppb1*Δ cells stained with calcofluor was examined. As already described, repression of *bgs1*$^+$ in the presence of sorbitol caused septation defects, but the cells remained viable for more than 60 hr. After 15 hr of repression, most cells contained one septum. At longer times (24 and 40 hr), most cells were multiseptated (Figures 2A and 2B). In contrast, *bgs1*$^+$ repression in either *ppb1*Δ or *pxl1*Δ cells caused a significant decrease in the number of septa (Figures 2A and 2B). These results indicate that CN, like paxillin (Cortés et al., 2015), collaborates with Bgs1 and plays an important role in septum synthesis and CAR ingression.

In cells lacking Pxl1 upon *bgs1*$^+$ repression, Ags1 and Bgs4, the main synthases of the cell wall and secondary septum, appeared in the cytoplasm, extended along the membrane, and did not concentrate at the septation area as they do in *bgs1*$^+$-repressed cells with Pxl1 (Cortés et al., 2015). Thus, the localization of either Ags1-GFP or GFP-Bgs4 synthases was analyzed in P*nmt81-bgs1*$^+$cells treated with the CN-specific inhibitor FK506 (5μg/mL) during the repression with thiamine. As in *pxl1*Δ cells, upon *bgs1*$^+$ repression (24 hr +T), both synthases appeared in the cytoplasm and extended along the plasma membrane of cells treated with the CN inhibitor (Figure 2C). These data suggest that CN, like Pxl1, cooperates with Bgs1 to concentrate in the division area the synthases required for the synthesis of the septum.

Pxl1 Binds to the Catalytic Subunit of CN and Is Required for Its Localization to the CAR

The above results strongly suggest that paxillin and CN function in the same signaling pathway. Therefore we analyzed the localization of both proteins during cytokinesis by performing time-lapse fluorescence microscopy in cells expressing Ppb1-GFP and mCherry-Pxl1. Although Pxl1 was detected earlier than Ppb1 (3–6 min), both localized to the CAR during cytokinesis (Figure 3A). Line scan analysis of red and green fluorescence confirmed that mCherry-Pxl1 and Ppb1-GFP co-localize (Figure 3B). Co-immunoprecipitation of endogenous HA-Pxl1 and Ppb1-GFP from yeast extracts confirmed that both proteins associate *in vivo* (Figure 3C).

Because Pxl1 appeared at the CAR slightly before Ppb1, we checked if Ppb1 localization was dependent on Pxl1. In most cells lacking Pxl1, Ppb1-GFP was not observed in the CAR, which was visualized using Rlc1-tdTomato. Only in a small percentage of *pxl1*Δ cells (7% [n = 165 cells]) with contracted rings, a faint signal of Ppb1-GFP with an intensity 10 times lower than in wild-type cells was observed (Figure 3D, arrows). Therefore CN localization to the CAR is mediated mainly by Pxl1, although other as yet unidentified proteins may contribute to localize CN to the CAR during late septation.

CN is a heterodimer composed of a catalytic and a regulatory subunit. In *Aspergillus fumigatus*, the CN catalytic subunit localizes at the hyphal septum independent of the regulatory subunit (Juvvadi et al., 2011). However, we observed that the catalytic subunit Ppb1-GFP was unable to localize to the CAR in the absence of Cnb1, the regulatory subunit of *S. pombe* CN (Figure 3E). Similarly, Cnb1-GFP did not localize to the ring in the absence of Ppb1 (Figure S1B). Additionally, in the absence of either subunit, there was no CN activity, as determined by using a strain carrying in the genome *GFP* under the control of *CDRE* (CN-dependent response element) as a reporter (Kume et al., 2011) (Figure S1C). These results suggest that CN activity is necessary for its localization to the CAR. Indeed, treatment of cells with FK506 during 6 hr caused disappearance of Ppb1-GFP from the CARs (Figure S1D).

To see if Pxl1 interacts with the catalytic or the regulatory subunit of CN, we performed *in vitro* pull-down assays with bacterially expressed GST or GST-Pxl1 and extracts from *S. pombe* cells expressing Ppb1-HA in the presence or absence of Cnb1, as well as extracts of cells expressing Cnb1-HA in the presence or absence of Ppb1 (Figure 3F). GST-Pxl1 pulled down Ppb1-HA from both wild-type and *cnb1*Δ extracts, whereas Cnb1-HA was pulled down only from wild-type extracts but not from *ppb1*Δ extracts (Figure 3F). These results indicate that paxillin binds to CN through the catalytic subunit Ppb1. Additionally, we used GST or GST-Pxl1 to pull-down MBP-Ppb1-HA purified from bacteria and proved a direct interaction between both proteins (Figure S1E).

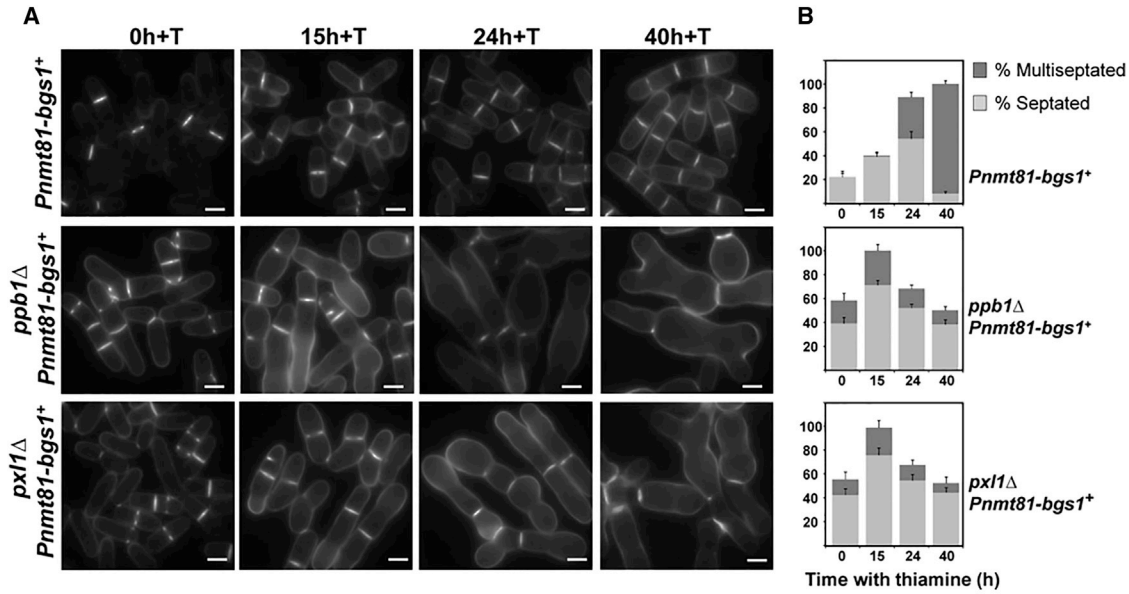

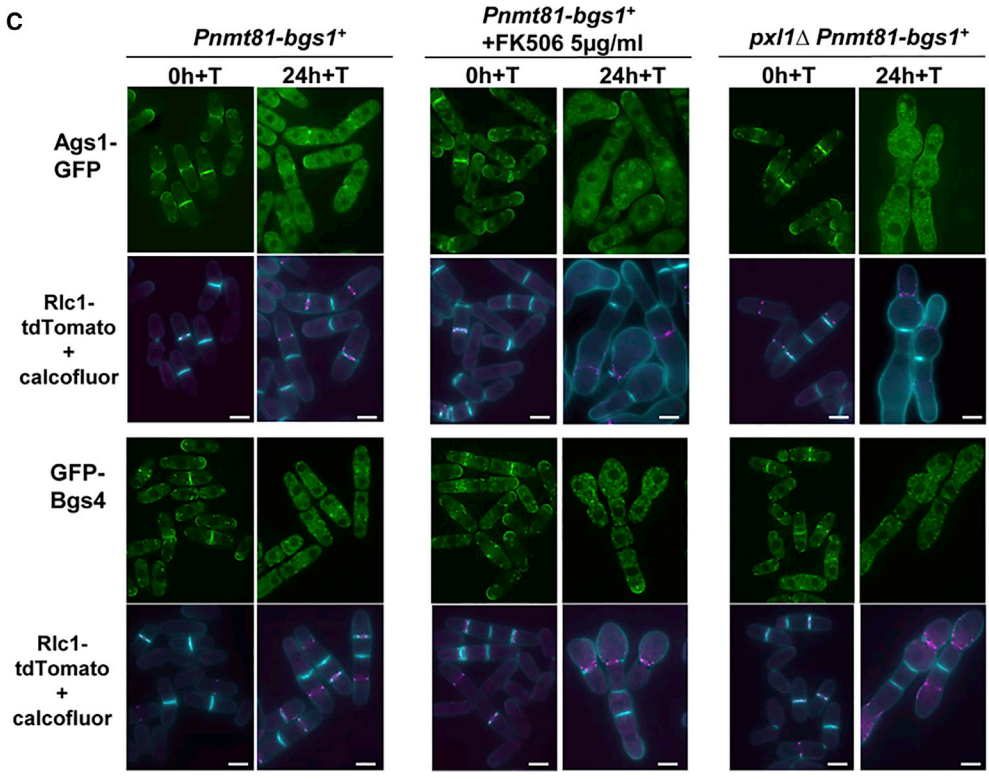

Figure 2. Calcineurin, as Paxillin, Collaborates with Bgs1 in Septum Formation

(A) Fluorescence micrographs of *Pnmt81-bgs1*$^+$, *ppb1*Δ *Pnmt81-bgs1*$^+$, and *pxl1*Δ *Pnmt81-bgs1*$^+$ cells stained with calcofluor. Cells were grown to early log phase in EMM + sorbitol and imaged at the indicated times after adding thiamine (+T) for *bgs1*$^+$ repression.

(B) Histograms showing the indicated percentages of septa in the strains used in (A); n = 150 cells or mycelial units for each time and strain; three technical replicates were made.

(C) Fluorescence micrographs of *Pnmt81-bgs1*$^+$ without or with FK506 (5 μg/mL), and *pxl1*Δ *Pnmt81-bgs1*$^+$ cells expressing Ags1-GFP and Rlc1-tdTomato (top) or GFP-Bgs4 Rlc1-tdTomato (bottom) and stained with calcofluor. Cells were grown as in (A) and imaged at the indicated times.

Scale bars, 5 μm.

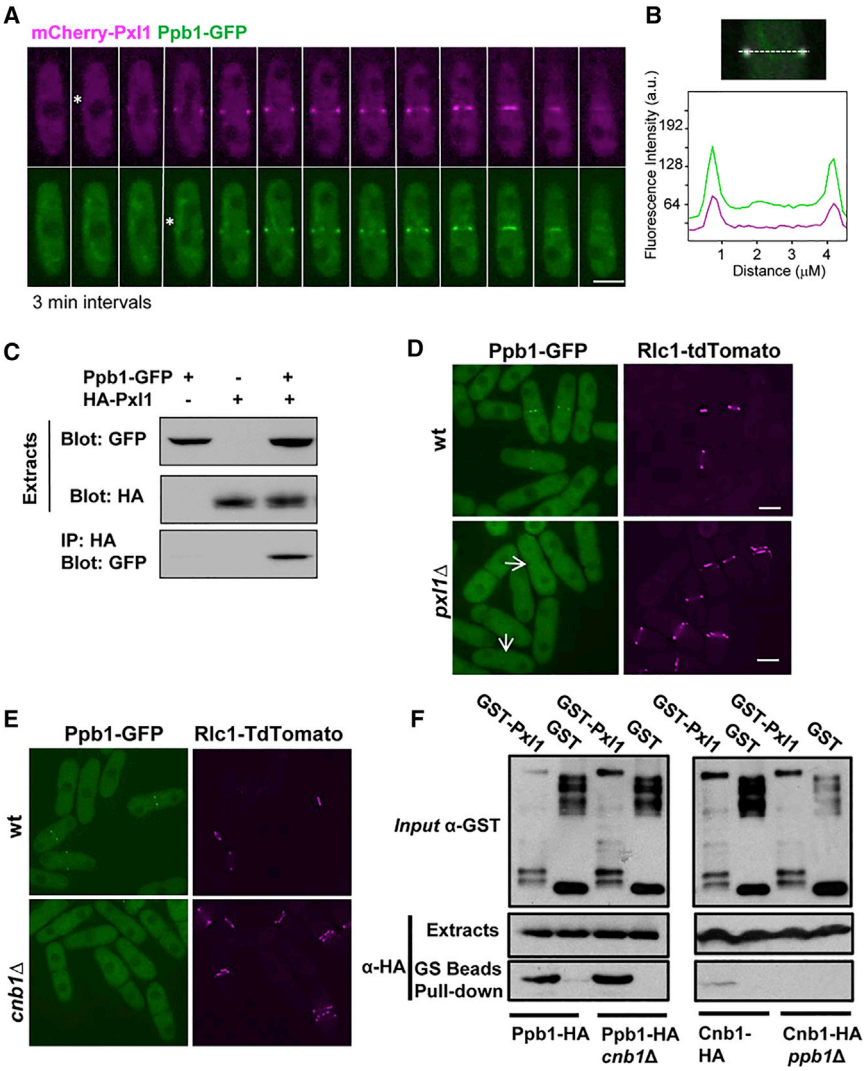

Figure 3. Pxl1 Binds to Calcineurin Catalytic Subunit and Is Required for Its Localization to the CAR

(A) Time-lapse fluorescence microscopy of cells endogenously expressing Ppb1-GFP and mCherry-Pxl1 to see the CAR localization of both proteins during cytokinesis. Asterisks indicate the first Pxl1 and Ppb1 detection at the ring.

(B) Line scan of mCherry-Pxl1 and Ppb1-GFP.

(C) Co-immunoprecipitation of endogenous HA-Pxl1 and Ppb1-GFP from yeast extracts.

(D) Fluorescence microscopy of wild-type (wt) and *pxl1*Δ cells expressing Ppb1-GFP and Rlc1-tdTomato. Arrows indicate Ppb1-GFP localization in late contraction rings of cells lacking *pxl1*$^{+}$.

(E) Fluorescence microscopy of wt and *cnb1*Δ cells expressing Ppb1-GFP and Rlc1-tdTomato. Scale bars, 5 μm. See also Figure S1B.

(F) *In vitro* interaction of Pxl1 and Ppb1. Bacterially expressed GST-Pxl1 was mixed with extracts of *ppb1-HA*, *cnb1Δ ppb1-HA*, *cnb1-HA*, and *ppb1Δ cnb1-HA* cells. GST-Pxl1 pull-down was done with glutathione-Sepharose beads and blotted with anti-HA antibodies. See also Figure S1C.

The N-Terminal 257 Amino Acid Residues and the C-Terminal LIM Domain of Pxl1 Are Necessary for CN Binding and Localization to the CAR

Pxl1 contains a N-terminal region with a polyproline motif that binds to Cdc15 SH3 domain and is responsible for the localization of Pxl1 to the CAR, and three LIM domains necessary for its function (Pinar et al., 2008; Roberts-Galbraith et al., 2009). To determine the contribution of Pxl1 domains to Ppb1 localization and function during cytokinesis, several truncated forms of Pxl1 (Figure 4A) were individually expressed in a *pxl1*Δ strain carrying Ppb1-GFP and Rlc1-tdTomato. We did not use the *GFP-pxl1ΔN* construct, which lacks the N terminus, because it does not localize to the CAR. On the basis of the Ppb1-GFP fluorescence intensity at the CAR (Figures 4B and 4C), we concluded that the C-terminal LIM domain was necessary for Ppb1 localization to the actomyosin ring. The strain lacking the C-terminal LIM domain had septation defects, although they were not as pronounced as the strain carrying the N-Pxl1 lacking the three LIM domains, which was similar to *pxl1*Δ strain (Pinar et al., 2008; Figure 4B).

CN recognizes its substrates primarily via two short linear motifs (SLiMs), PxIxIT, and LxVP. Multiple degenerate PxIxIT motifs exist, and the hydrophobic residues at positions 3 and 5 or the hydrophilic residue at position 6 is not always a perfect match (Aramburu et al., 1998; Roy and Cyert, 2009). Analysis of Pxl1 sequence identifies two possible CN docking motifs located in the N-terminal region (PTLPLQ; amino acids 181–186) and in the C-terminal LIM domain (PILGIS; amino acids 384–389). Mutation of these amino acids to alanine (Pxl1-M3 and Pxl1-M4, respectively) verified that PILGIS amino acids at the LIM domain were necessary for the localization of CN to the CAR and for the function of Pxl1. On the other hand, PTLPLQ motif at the N-terminal region was not required (Figures 4B and 4C).

Pxl1 interaction with Ppb1 was also studied by using bacterially expressed GST fusions of the different Pxl1 fragments and *S. pombe* extracts expressing Ppb1-HA. Pull-down assays of GST fusions with glutathione Sepharose beads showed that the N-terminal half of Pxl1, but not the PTLPLQ motif, was necessary for the binding of Pxl1 to Ppb1 and confirmed that the C-terminal LIM domain and its PILGIS motif participated in the binding of Pxl1 to Ppb1 (Figure 4D).

Artificial Localization of Ppb1 to the CAR Suppresses *pxl1Δ ppb1Δ* Cytokinesis Defects

Our results indicate that Pxl1 links CN to the CAR. If this is the major function of Pxl1, we predict that the LIM domains might be dispensable if Ppb1 is artificially bound to the N-terminal part of Pxl1 in order to reach the CAR. We constructed a chimeric

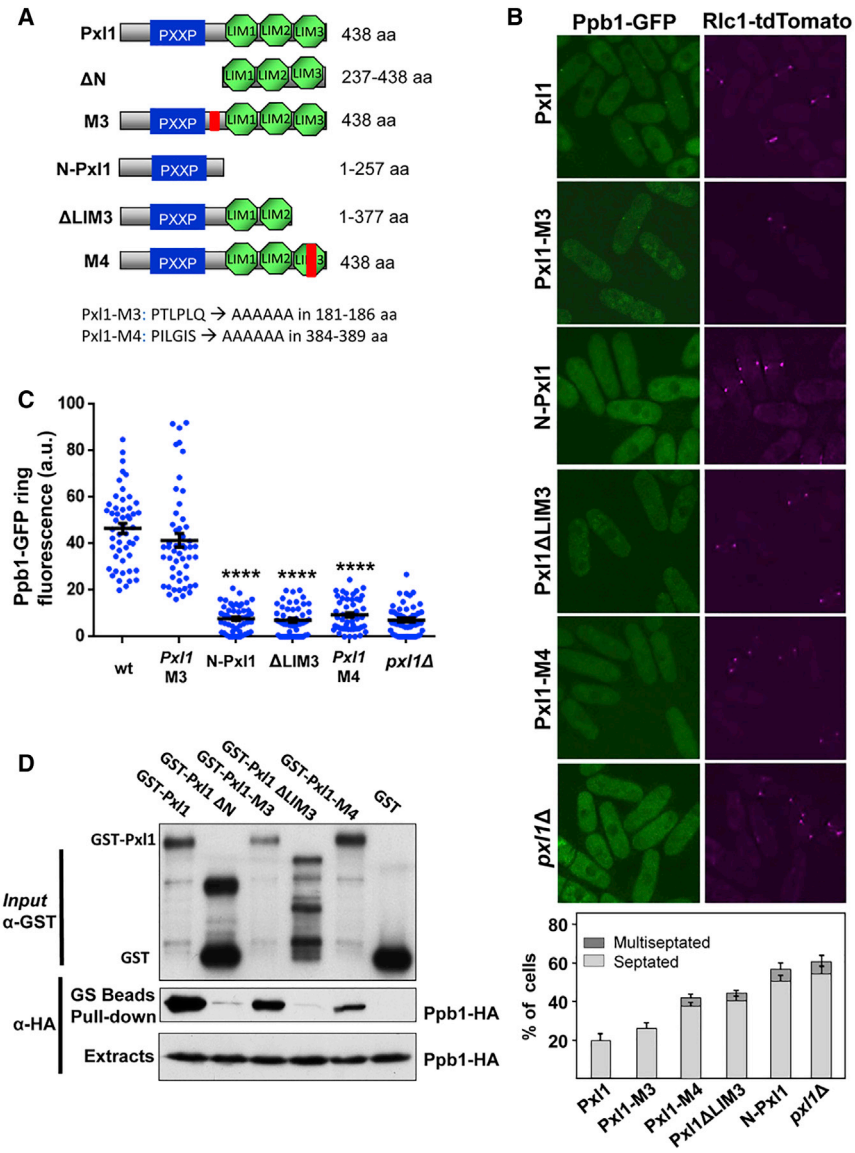

Figure 4. Pxl1 N-Terminal 257 Amino Acid Residues and C-Terminal LIM3 Domain Are Necessary for Ppb1 Binding and Localization to the CAR

(A) Schematic representation of Pxl1domains and the different truncations and/or mutations generated.

(B) Fluorescence micrographs of wild-type (wt), *pxl1*Δ, and cells expressing different Pxl1 versions. The histogram represent percentages of septating and multiseptated cells in these strains (n = 150 cells for each strain; three technical replicates were performed). Scale bar, 5 μm.

(C) Ppb1-GFP fluorescence intensity (a.u.) at the ring in the cells expressing truncated or mutated Pxl1. Only cells with the ring expanding the cell diameter were measured; n = 25 cells for each strain. Black lines indicate mean ± SEM. ****p < 0.0001 (two-way ANOVA).

(D) Interaction of Pxl1 truncations and Ppb1. Extracts from cells expressing Ppb1-HA were pulled down with truncated or mutated Pxl1 produced as GST fusion in bacteria and GS beads. Input blotted with anti-GST (top), GS pull-down (middle), and total Ppb1-HA in cell extracts (bottom) blotted with anti-HA antibody.

protein containing GFP-N-Pxl1 (1–257 amino acids) fused to Ppb1. This chimera was expressed from the native *pxl1*$^{+}$ promoter (Figure 5A), which depends on the Ace2 transcription factor. Ace2 activates transcription during the M-G1 transition and cytokinesis (Rustici et al., 2004). As previously described, expression of GFP-N-Pxl1 alone did not correct the cytokinesis defect of a *pxl1*Δ strain (Pinar et al., 2008) and did not localize GFP-Ppb1 (Figure 4B). In contrast, the GFP-N-Pxl1-Ppb1 chimera restored Ppb1 localization to the CAR and suppressed the multiseptation phenotype of a *pxl1*Δ *ppb1*Δ double-mutant strain (Figures 5B and 5C). Therefore, the GFP-N-Pxl1-Ppb1 chimera suppresses the defects of cells lacking the paxillin LIM domains and the CN catalytic subunit. When we expressed *GFP-N-pxl1-ppb1* in *pxl1*Δ *ppb1*Δ *cnb1*Δ cells lacking both subunits of CN, GFP-N-Pxl1-Ppb1 still localized to the CAR, but because of the lack of CN activity, there was no suppression of the cytokinesis defects (Figures 5B and 5C).

Expression of the GFP-N-Pxl1-Ppb1 caused other defects, such as misshapen cells and abnormal cell wall accumulations that stained with calcofluor (Figure 5B). Additionally, some fluorescent dots of GFP-N-Pxl1-Ppb1 were observed at the cortex of cells already separated, while GFP-N-Pxl1 was never detected in the cells that completed septation and initiated septum degradation (Figure S2A). These defects were also present when the chimera was expressed in wild-type cells with endogenous Pxl1 and Ppb1 (Figure S2B), suggesting that the cause could be an excess of CN activity. Indeed, there were no abnormal cell wall accumulations in *pxl1*Δ *ppb1*Δ *cnb1*Δ cells expressing the chimera, with no CN activity (Figure 5B). All the phenotypes caused by the GFP-N-Pxl1-Ppb1 chimera were independent of the CN-dependent Prz1 transcription factor because *pxl1*Δ *ppb1*Δ *prz1*Δ triple-mutant cells displayed the same phenotype as cells expressing the chimera in the presence of Prz1 (Figure S2C).

To circumvent the problem of excessive CN activity, we used FK506. Addition of this inhibitor (5 μg/mL) to wild-type cells during 12 hr resulted in a phenotype identical to that of CN-deleted cells (Yoshida et al., 1994; Sugiura et al., 1998; Figure S2D). In contrast, addition of FK506 (5 μg/mL, 12 hr) to *GFP-N-pxl1-ppb1 pxl1*Δ *ppb1*Δ cells eliminated the cell wall accumulations, and morphology defects and cells were similar to wild-type (Figures 5B and 5C). When the FK506 concentration was raised to 20 μg/mL, the cells expressing the chimera presented cytokinesis defects similar to those of *pxl1*Δ *ppb1*Δ strain (Figure S2D).

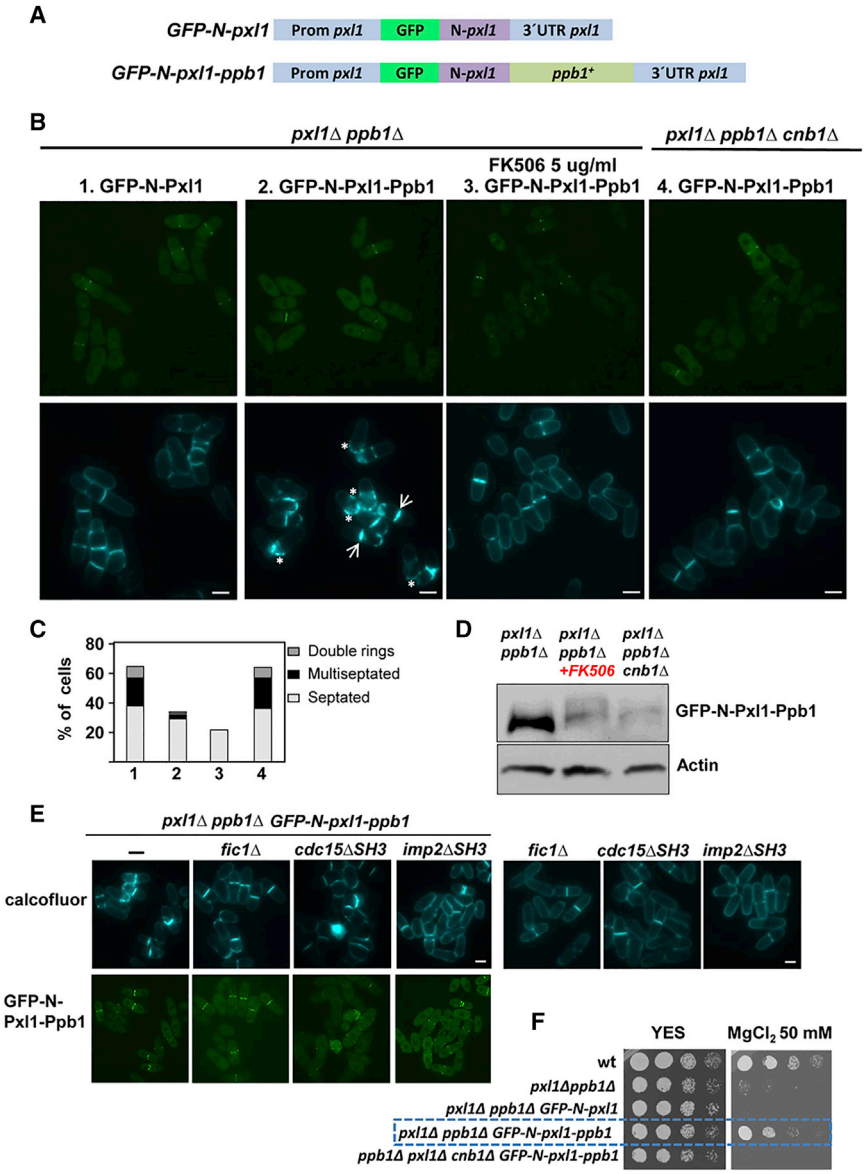

Figure 5. Artificial Localization of Ppb1 to the CAR Suppresses *pxl1Δ* Cytokinesis Defects

(A) Schematic representation of *GFP-N-pxl1* (control) and *GFP-N-pxl-ppb1* constructs used to link calcineurin to the CAR.

(B) Fluorescence micrographs of calcofluor-stained (bottom) *pxl1Δ ppb1Δ* and *pxl1Δ ppb1Δ cnb1Δ* cells carrying GFP-N-Pxl1 or GFP-N-Pxl1-Ppb1 fusion. Arrows indicate aberrant septa with a thicker area at the center. Asterisks point to abnormal accumulations of calcofluor-stained material.

(C) Quantification of the phenotypes observed in (B) (n = 275 cells for each strain or condition).

(D) Western blot analysis of GFP-N-Pxl1-Ppb1 protein expressed in *pxl1Δ ppb1Δ* cells untreated or treated with FK506 (20 μg/mL) or in *pxl1Δ ppb1Δ cnb1Δ* cells. Lysates were run in 6% acrylamide PhosTag gels (37.5 μM) and probed with anti-GFP antibodies. Actin was used as a loading control.

(E) Fluorescence images from cells of the indicated genotype expressing the GFP-N-Pxl1-Ppb1 chimera and stained with calcofluor. Single *fic1Δ*, *cdc15ΔSH3*, and *imp2ΔSH3* mutant cells stained with calcofluor are also shown.

(F) Cells of the indicated genotype expressing *GFP-N-pxl1* or *GFP-N-pxl1-ppb1* were grown in YES medium at 28°C and spotted on plates with the same medium without or with $MgCl_2$ (50 mM) at OD_{600} 2 and 1:4 serial dilutions. Plates were incubated for 2–3 days at 28°C.

Scale bars, 5 μm. See also Figure S2.

CN is a phosphoprotein, and it has been reported that under certain conditions it can undergo autodephosphorylation, resulting in higher phosphatase activity (Hashimoto et al., 1988). Treatment of cells expressing Ppb1-GFP with FK506 during 4 hr already caused an accumulation of the hyperphosphorylated form of this phosphatase (Figure S2E). Similarly, the chimeric GFP-N-Pxl1-Ppb1 protein showed reduced electrophoretic mobility in *pxl1Δ ppb1Δ* extracts from cells treated with FK506 (20 μg/mL, 4 hr) or in *pxl1Δ ppb1Δ cnb1Δ* cell extracts, lacking phosphatase activity (Figure 5D). Together, these results suggest that there is an excess of CN phosphatase activity in the cells expressing the chimeric protein N-Pxl1-Ppb1.

Expression of the GFP-N-Pxl1-Ppb1 chimera was sufficient to suppress the synthetic lethality of *pxl1Δ ppb1Δ* with *fic1Δ*, *cdc15ΔSH3*, or *imp2ΔSH3* (Figure 5E). The triple-mutant strains expressing the chimera presented a phenotype similar to the parental single mutant strains, *fic1Δ*, *cdc15ΔSH3*, and *imp2ΔSH3*, indicating that an excess of CN activity could not suppress other defects of these mutants. Expression of the chimera was also sufficient to suppress the $MgCl_2$ sensitivity of *pxl1Δ ppb1Δ* double-mutant cells (Figure 5F). In summary, the functional defects of *pxl1Δ* and *ppb1Δ* can be rescued by artificial linkage of Ppb1 to the CAR, suggesting that the main function of Pxl1 LIM domains is to link CN to the CAR.

CN Is Necessary for the Concentration of Pxl1 at the CAR

Pxl1 concentration at the CAR rises during contraction (Cortés et al., 2015). We have shown here that Pxl1 mediates the localization of Ppb1 to the CAR. To see if the opposite also occurred and Ppb1 was necessary for Pxl1 localization and/or concentration, we quantified the GFP-Pxl1 fluorescence in wild-type and *ppb1Δ* cells at three different stages of septation: early septa (<0.6 μm), middle septa (0.6–1.2 μm), and advanced septa (>1.2 μm). As previously described (Cortés et al., 2015), in wild-type cells GFP-Pxl1 fluorescence at the CAR increased from the onset of septation until the completion of the septum

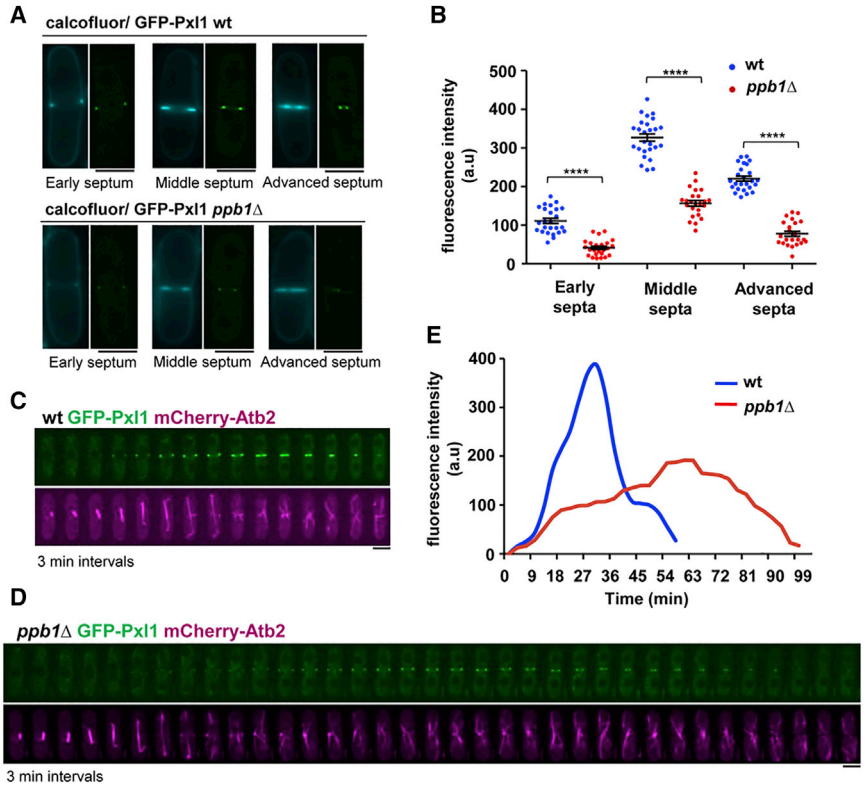

Figure 6. Calcineurin Activity Is Necessary for Paxillin Concentration at the CAR

(A) Fluorescence images showing representative cells at different stages of septation (early, middle, and late) of wild-type or *ppb1Δ* strains expressing GFP-Pxl1 and stained with calcofluor.

(B) GFP-Pxl1 fluorescence intensity in these strains at different stages of septation. Black lines indicate mean ± SEM; n = 25 cells for each condition and strain. ****p < 0.0001 (Student's t test).

(C and D) Time-lapse images (3 min intervals) from wild-type (C) and *ppb1Δ* (D) cells expressing GFP-Pxl1 and mCherry-Atb2 are shown. Spindle microtubules appearance is used to stablish time 0.

(E) Total GFP-Pxl1 fluorescence was quantified along the time in cells shown in (C) and (D).

Scale bars, 5 μm.

(Figures 6A and 6B). This accumulation of Pxl1 at constricting rings was lower in cells lacking CN (Figures 6A and 6B). Time-lapse analysis of wild-type and *ppb1*Δ cells carrying GFP-Pxl1 and mCherry-Atb2 confirmed the results obtained in septating cells at different stages (Figures 6C and 6D). The maximum GFP-Pxl1 fluorescence intensity detected in *ppb1*Δ cells was 50% lower than in wild-type cells. In addition, the progression of ring contraction and septation was noticeably slower in *ppb1*Δ cells, and the maximum GFP-Pxl1 fluorescence intensity was reached with a 30 min delay respect to wild-type cells (Figure 6E). These results uncover a positive feedback loop in which paxillin is required to bring CN to the CAR, and in turn CN promotes the concentration of paxillin in this structure.

CN Activity Causes *In Vivo* and *In Vitro* Dephosphorylation of the F-BAR Protein Cdc15

Concentration of Pxl1 at the CAR requires its binding to the SH3 domain of the F-BAR protein Cdc15 (Cortés et al., 2015). This scaffold protein binds many partners and plays a key role in organizing the CAR (Ren et al., 2015). Because Cdc15 dephosphorylation stimulates its scaffolding activity (Roberts-Galbraith et al., 2010), we considered that CN might dephosphorylate Cdc15. Co-immunoprecipitation experiments showed that Ppb1 interacted *in vivo* with Cdc15 in cells synchronized in cytokinesis (Figure 7A). Hence we analyzed the phosphorylation state of Cdc15 in cells with different levels of CN activity. We treated cells expressing GFP-Cdc15 with FK506 to inhibit CN. In addition, we used GFP-Cdc15 cells expressing the N-Pxl1-Ppb1 chimera to analyze Cdc15 phosphorylation under an excess of CN activity. Asynchronous cultures of wild-type and *pxl1*Δ *ppb1*Δ *N-pxl1-ppb1* cells expressing GFP-Cdc15, untreated and treated with FK506 for 2 hr, already displayed changes in GFP-Cdc15 electrophoretic mobility. There was a hyperphosphorylated form in both types of FK506-treated cells and a hypophosphorylated form in cells expressing *N-pxl1-ppb1* (Figure 7B). These observations suggested that CN phosphatase was regulating Cdc15 phosphorylation status.

Cdc15 becomes dephosphorylated as cells progress through mitosis (Fankhauser et al., 1995; Clifford et al., 2008) with maximum Cdc15 dephosphorylation during anaphase and Cdc15 phosphorylation reestablished upon septation. We analyzed GFP-Cdc15 phosphorylation dynamics during mitosis and cytokinesis in cells without or with FK506 to inhibit CN. Synchronous cultures were generated by using a *cdc25-22* strain arrested in G2 at 36°C during 4 hr and released at 25°C. FK506 (5 μg/mL) was added at the beginning of the arrest. GFP-Cdc15 from FK506-treated cells appeared hyperphosphorylated at the time of culture release (0 min) (Figure 7C). Sixty minutes later, GFP-Cdc15 was slightly dephosphorylated but not to the same extent as in untreated cells (Figure 7C). These results suggest that Cdc15 dephosphorylation during cytokinesis depends partially on CN phosphatase activity, although other phosphatases could be involved as well. Upon septation (90 min after culture release), GFP-Cdc15 was rephosphorylated in wild-type cells, reaching the maximum phosphorylation status at 120 min. In FK506-treated cells, Cdc15 phosphorylation reestablishment seemed to be slightly delayed with respect to control cells (Figure 7C). This delay in the absence of CN activity is coincident with a delay in septation in these cells. Currently we cannot determine if it is the cause or the consequence of the septation delay.

In *cdc25-22*-synchronous cultures expressing *N-pxl1-ppb1*, we observed that at time 0 after culture release, Cdc15 was already hypophosphorylated compared with wild-type cells. At

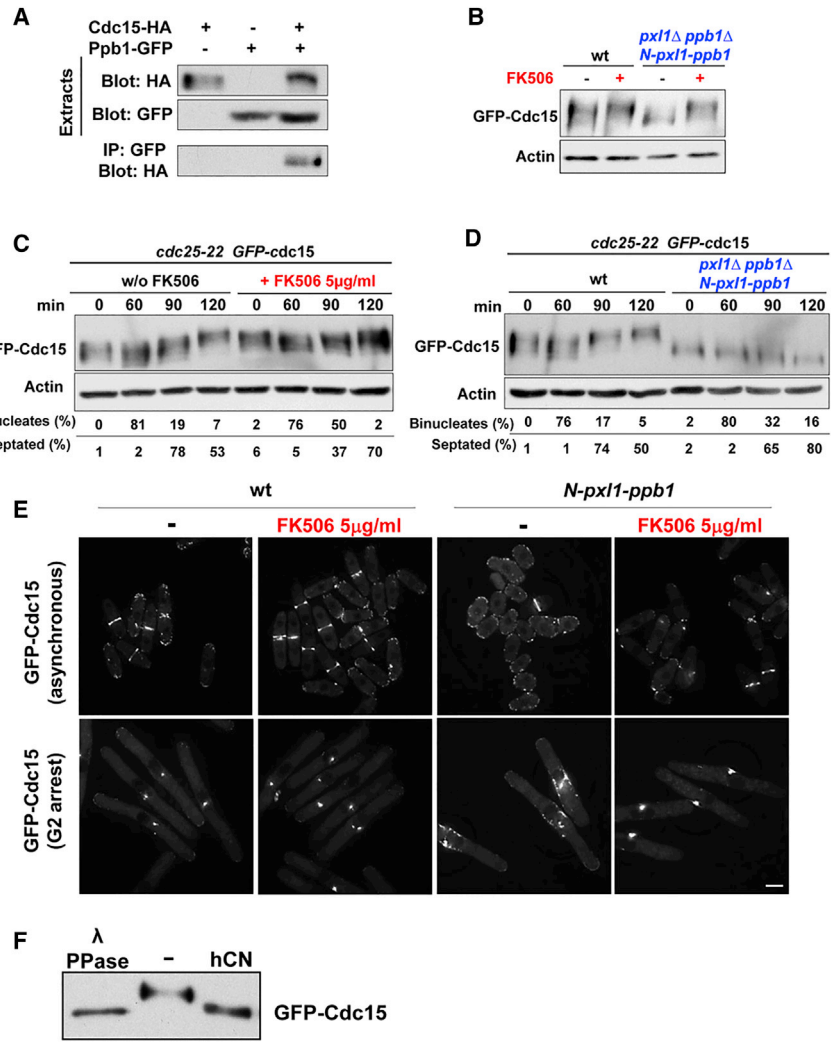

Figure 7. Calcineurin Activity Causes *In Vivo* and *In Vitro* Dephosphorylation of the F-BAR Protein Cdc15

(A) Co-immunoprecipitation of endogenously tagged Cdc15-HA and Ppb1-GFP from yeast extracts of cdc25-22 synchronic cultures, obtained 60 min after cultures release at 25°C. Immunoprecipitation was performed with anti-GFP antibodies and immunoblotting with anti-HA antibodies.

(B) Protein extracts form asynchronous cultures of cells expressing GFP-Cdc15 in a wild-type strain or both GFP-Cdc15 and the chimeric protein N-Pxl1-Ppb1 in a *pxl1Δppb1Δ* strain, treated or not with FK506 (20 μg/mL) for 2 hr, were analyzed by western blot using anti-GFP and anti-actin antibodies.

(C) Protein extracts from *cdc25-22* GFP-Cdc15 synchronous cultures, treated or not with FK506. Mid-log phase cells were shifted to 36°C for 4 hr and then released to permissive temperature (25°C). At the indicated times after release, samples were analyzed by western blot as in (B). Percentage of binucleates and septation index are included to monitor cell cycle progression and septation.

(D) Protein extracts from *cdc25-22 GFP-Cdc15* or *cdc25-22 GFP-Cdc15 pxl1Δ ppb1Δ N-pxl1-ppb1* cells collected at different time points after release were analyzed by western blot as in (B). Progression of mitosis and cytokinesis was determined as in (C).

(E) Live cell images of asynchronous or G2-arrested cultures of wild-type or *pxl1Δ ppb1Δ N-pxl1-ppb1* strains, treated or not with FK506 5 μg/mL. Scale bar, 5 μm.

(F) Immunopurified GFP-Cdc15 protein obtained from *cdc25-22 GFP-Cdc15* synchronized cultures blocked during 4 hr at 36°C and released during 1 hr at 25°C in the presence of FK506 (5 μg/mL) was treated with λ phosphatase, buffer, or human recombinant calcineurin (CN) and analyzed by western blot using anti-GFP antibodies.

60 min after release, Cdc15 was also more dephosphorylated, and rephosphorylation upon septation (90 and 120 min after release) did not occur in these cells (Figure 7D). We have described above that the N-Pxl1-Ppb1 chimera remained at the division site once septation was completed, whereas in wild-type cells, Pxl1 and Ppb1 disappeared from the cell equator after septum completion. Thus, the remnant CN phosphatase activity in cells expressing the chimera could be impeding Cdc15 rephosphorylation after septation.

A mutated Cdc15 constitutively hypophosphorylated displays precocious medial localization in G2-arrested cells (Roberts-Galbraith et al., 2010). To corroborate the role of CN in Cdc15 dephosphorylation, we analyzed the localization of GFP-Cdc15 in wild-type and *pxl1Δ ppb1Δ N-pxl1-ppb1* cells with or without FK506. GFP-Cdc15 localized as dots at the cell tips in interphase and as a single bigger dot in the cytoplasm of G2-arrested wild-type cells. In contrast, in asynchronous *N-pxl1-ppb1*-expressing cells with an excess of CN activity, GFP-Cdc15 dots were not restricted at the cell tips but were dispersed all around the cell cortex (Figure 7E). In G2-arrested cultures of these cells, GFP-Cdc15 was abnormally localized to the middle of the cell cortex, similar to what was reported for dephosphorylated mutant forms of Cdc15 (Roberts-Galbraith et al., 2010).

No change in GFP-Cdc15 localization was observed upon treatment of wild-type cells with FK506 (5 μg/mL, 4 hr) (Figure 7E). In agreement, Cdc15 hyperphosphorylated mutant forms did not change their localization either in asynchronous or G2-arrested cells (Roberts-Galbraith et al., 2010). However, in both asynchronous and G2-arrested cultures of cells expressing *N-pxl1-ppb1*, the FK506 treatment (5 μg/mL, 4 hr) changed Cdc15 localization to that of wild-type cells. GFP-Cdc15 dots were restricted to the cell tips in interphase, and a single cytoplasmic dot appeared in G2-arrested cultures (Figure 7E). In summary, our findings suggest that CN phosphatase activity is needed for the proper Cdc15 phosphorylation dynamics and localization.

We next analyzed if CN dephosphorylates Cdc15 *in vitro*. GFP-Cdc15 was immunopurified from *cdc25-22*-synchronized

cultures in anaphase in the presence of FK506 and was treated with λ phosphatase or human recombinant CN. In both cases Cdc15 exhibited increased mobility compared with the untreated protein (Figure 7F). These results demonstrate that Cdc15 is a phosphoprotein and a substrate of CN. However, the possibility that *in vivo* a different phosphatase works directly on Cdc15 is not excluded.

DISCUSSION

CN is the main eukaryotic cell transducer of signals generated by changes in Ca^{2+} levels (Li et al., 2011). This phosphatase plays important roles in different processes, ranging from stress response survival in fungi (Juvvadi and Steinbach, 2015) to mammalian development (Graef et al., 2001). Fission yeast CN regulates multiple biological processes, including cytokinesis (Sugiura et al., 2002). Although CN localization is mainly cytoplasmic, it was also observed at the CAR (McDonald et al., 2017). We show here that CN localizes to the CAR once it is formed, constricts with the ring, and remains there until the end of septation. We confirmed previous reports (Fujita et al., 2002; Cadou et al., 2013) and analyzed in detail the cytokinesis defects caused by the absence of CN, finding a strong similarity with the defects detected in cells lacking Pxl1 (Ge and Balasubramanian, 2008; Pinar et al., 2008; Cortés et al., 2015). Moreover, our results indicate that Pxl1 links CN to the CAR and reveal the importance of CN signaling in the connection between CAR contraction and septum biosynthesis. Thus, the phenotype of cells depleted of Bgs1 in the absence of either CN or Pxl1 is similar and indicates that both collaborate with Bgs1 in the fission yeast septum ingression.

Pxl1 binds directly to the catalytic subunit of CN, and its major function is the localization of this phosphatase to the CAR because artificial localization of Ppb1 to the CAR fused to the N-terminal domain of Pxl1 can substitute the function of Pxl1 LIM domains. Cells expressing the N-Pxl1-Ppb1 chimera have morphological defects, likely because of the ectopic hyperactivity of CN, as FK506 could suppress them, making the cells similar to wild-type cells. Previous studies showed that simultaneous overexpression of constitutively active Ppb1ΔC and Cnb1 causes cell wall accumulations and aberrant morphology similar to that observed in cells expressing N-Pxl1-Ppb1 and that these defects are also suppressed by the addition of FK506 (Sio et al., 2005). The N-Pxl1-Ppb1 fusion may activate CN or facilitate the binding to its substrates, making the phosphatase more efficient. It may also stabilize CN localization during cytokinesis, extending its function after the end of cytokinesis.

We have shown here that Pxl1 connects CN to the CAR and that CN activity is necessary to allow Pxl1 concentration at the CAR. This positive feedback loop between both proteins could be mediated by regulation of Cdc15 phosphorylation. Indeed, we described that CN affected Cdc15 phosphorylation dynamics. The absence of CN activity altered Cdc15 phosphorylation in a manner reminiscent of that described for the absence of the phosphatase Clp1 (Wachtler et al., 2006; Clifford et al., 2008). Likely both phosphatases collaborate in Cdc15 dephosphorylation during cytokinesis. In the absence of CN activity, Cdc15 was always hyperphosphorylated. This would be in agreement with lower concentration of Cdc15 binding partners at the cell equator (Roberts-Galbraith et al., 2010). In fact, Pxl1 is a Cdc15 binding partner (Roberts-Galbraith et al., 2009), and CN activity is needed for Pxl1 concentration at the CAR. Moreover, Fic1, another Cdc15 binding partner, also required CN activity to concentrate at the CAR (Figure S3).

The function of paxillin in the signaling of CN could be conserved in other ascomycetes, such as *A. nidulans*. In this fungus, CN signaling regulates cytokinesis and hyphal growth (Steinbach et al., 2006), and CN localization to the hyphal septum is required for the correct deposition of new cell wall material (Juvvadi et al., 2011). However, how CN binds to the septum in *Aspergillus* remains unclear. In the basidiomycete *C. neoformans*, CN controls septum positioning and cell separation in coordination with Cts1 (Fox et al., 2003; Aboobakar et al., 2011). This protein presents similarity to *S. pombe* Fic1 (Aboobakar et al., 2011), and *fic1*$^{+}$ deletion is synthetically lethal with either *pxl1*Δ or *ppb1*Δ (Roberts-Galbraith et al., 2009), suggesting that the signaling of these molecules during cytokinesis might be conserved.

In mammalian cells, CN is required during the abscission stage of cytokinesis and is specifically localized to the midbody region (Chircop et al., 2010). Interestingly, one of the three human catalytic subunits of CN, PPP3CA, interacts with a LIM and SH3 domain protein, LASP1 (Q14847, UniProt), important for the regulation of actin-based cytoskeletal activities, according to the Human DEPhOsphorylation Database (www.depod.org). Perhaps there is a conserved interaction between the CN catalytic subunit and LIM domains, as we have proved in this work that the C-terminal LIM domain of Pxl1 is necessary for its binding to Ppb1.

A systematic study using bioinformatics and phosphoproteomics in *S. cerevisiae* identified many new CN targets (Goldman et al., 2014). Our data reinforce the importance of CN signaling in the regulation of cytokinesis through targets different from the transcription factor Prz1. Similarly, in *Aspergillus*, CN signaling in cytokinesis and hyphal growth is only partly dependent on the transcription factor CrzA homologous to Prz1, indicating that other CN effectors are required for cytokinesis (Cramer et al., 2008; Soriani et al., 2008; Juvvadi et al., 2017). The molecular events that occur during cytokinesis require activation and inactivation of relevant signaling pathways, likely through phosphorylation and dephosphorylation of different proteins. This study shows that CN contributes to fission yeast cytokinesis through paxillin-mediated binding to the CAR. In this way CN can reach other proteins, such as Cdc15, which binds within the N terminus of paxillin. Future studies will be directed toward unveiling other elements of this network.

STAR★METHODS

Detailed methods are provided in the online version of this paper and include the following:

- KEY RESOURCES TABLE
- CONTACT FOR REAGENT AND RESOURCE SHARING
- EXPERIMENTAL MODEL AND SUBJECT DETAILS
  - Fission yeast growth conditions

SUPPLEMENTAL INFORMATION

Supplemental Information includes three figures and one table and can be found with this article online at https://doi.org/10.1016/j.celrep.2018.09.062.

ACKNOWLEDGMENTS

We thank J. Cansado and J.C. Cortés for thoughtful comments and D.M. Posner for language revision. Thanks to J.M. Márquez and E. Portales for technical help. We thank K. Gould, T. Pollard, J.Q. Wu, D. Hirata, and Q. Jin for generous gifts of strains and plasmids. This work was supported by grants BIO2015-69958-P from the Ministerio de Economía y Competitividad and CSI068P17 from the Junta de Castilla y León, Spain, and by the European Regional Development Fund (FEDER). V.A. acknowledges support through a contract from Junta de Castilla y León and the European Social Fund.

AUTHOR CONTRIBUTIONS

R.M.-G., V.A., P.M.C., and P.P. conceived and designed the study and analyzed the data. R.M.-G., V.A., and P.M.C. performed most experiments. R.A.V., M.P., S.A.R., J.C.-B., and J.C.R. collaborated on some experiments. R.M.-G. and P.P. wrote the paper.

DECLARATION OF INTERESTS

The authors declare no competing interests.

Received: March 16, 2018
Revised: August 1, 2018
Accepted: September 19, 2018
Published: October 16, 2018

REFERENCES

Aboobakar, E.F., Wang, X., Heitman, J., and Kozubowski, L. (2011). The C2 domain protein Cts1 functions in the calcineurin signaling circuit during high-temperature stress responses in Cryptococcus neoformans. Eukaryot. Cell *10*, 1714–1723.

Adler, A., Park, Y.D., Larsen, P., Nagarajan, V., Wollenberg, K., Qiu, J., Myers, T.G., and Williamson, P.R. (2011). A novel specificity protein 1 (SP1)-like gene regulating protein kinase C-1 (Pkc1)-dependent cell wall integrity and virulence factors in Cryptococcus neoformans. J. Biol. Chem. *286*, 20977–20990.

Aramburu, J., Garcia-Cózar, F., Raghavan, A., Okamura, H., Rao, A., and Hogan, P.G. (1998). Selective inhibition of NFAT activation by a peptide spanning the calcineurin targeting site of NFAT. Mol. Cell *1*, 627–637.

Arasada, R., and Pollard, T.D. (2014). Contractile ring stability in S. pombe depends on F-BAR protein Cdc15p and Bgs1p transport from the Golgi complex. Cell Rep. *8*, 1533–1544.

Cadou, A., Couturier, A., Le Goff, C., Xie, L., Paulson, J.R., and Le Goff, X. (2013). The Kin1 kinase and the calcineurin phosphatase cooperate to link actin ring assembly and septum synthesis in fission yeast. Biol. Cell *105*, 129–148.

Carnahan, R.H., and Gould, K.L. (2003). The PCH family protein, Cdc15p, recruits two F-actin nucleation pathways to coordinate cytokinetic actin ring formation in *Schizosaccharomyces pombe*. J. Cell Biol. *162*, 851–862.

Cheng, H., Sugiura, R., Wu, W., Fujita, M., Lu, Y., Sio, S.O., Kawai, R., Takegawa, K., Shuntoh, H., and Kuno, T. (2002). Role of the Rab GTP-binding protein Ypt3 in the fission yeast exocytic pathway and its connection to calcineurin function. Mol. Biol. Cell *13*, 2963–2976.

Chircop, M., Malladi, C.S., Lian, A.T., Page, S.L., Zavortink, M., Gordon, C.P., McCluskey, A., and Robinson, P.J. (2010). Calcineurin activity is required for the completion of cytokinesis. Cell. Mol. Life Sci. *67*, 3725–3737.

Clifford, D.M., Wolfe, B.A., Roberts-Galbraith, R.H., McDonald, W.H., Yates, J.R., 3rd, and Gould, K.L. (2008). The Clp1/Cdc14 phosphatase contributes to the robustness of cytokinesis by association with anillin-related Mid1. J. Cell Biol. *181*, 79–88.

Cortés, J.C., Konomi, M., Martins, I.M., Muñoz, J., Moreno, M.B., Osumi, M., Durán, A., and Ribas, J.C. (2007). The (1,3)beta-D-glucan synthase subunit Bgs1p is responsible for the fission yeast primary septum formation. Mol. Microbiol. *65*, 201–217.

Cortés, J.C., Sato, M., Munoz, J., Moreno, M.B., Clemente-Ramos, J.A., Ramos, M., Okada, H., Osumi, M., Duran, A., and Ribas, J.C. (2012). Fission yeast Ags1 confers the essential septum strength needed for safe gradual cell abscission. J. Cell Biol. *198*, 637–656.

Cortés, J.C., Pujol, N., Sato, M., Pinar, M., Ramos, M., Moreno, B., Osumi, M., Ribas, J.C., and Pérez, P. (2015). Cooperation between paxillin-like protein Pxl1 and glucan synthase Bgs1 is essential for actomyosin ring stability and septum formation in fission yeast. PLoS Genet. *11*, e1005358.

Cramer, R.A., Jr., Perfect, B.Z., Pinchai, N., Park, S., Perlin, D.S., Asfaw, Y.G., Heitman, J., Perfect, J.R., and Steinbach, W.J. (2008). Calcineurin target CrzA regulates conidial germination, hyphal growth, and pathogenesis of Aspergillus fumigatus. Eukaryot. Cell *7*, 1085–1097.

Cyert, M.S. (2001). Genetic analysis of calmodulin and its targets in Saccharomyces cerevisiae. Annu. Rev. Genet. *35*, 647–672.

Fang, Y., Imagawa, K., Zhou, X., Kita, A., Sugiura, R., Jaiseng, W., and Kuno, T. (2009). Pleiotropic phenotypes caused by an opal nonsense mutation in an essential gene encoding HMG-CoA reductase in fission yeast. Genes Cells *14*, 759–771.

Fankhauser, C., Reymond, A., Cerutti, L., Utzig, S., Hofmann, K., and Simanis, V. (1995). The S. pombe cdc15 gene is a key element in the reorganization of F-actin at mitosis. Cell *82*, 435–444.

Fox, D.S., Cox, G.M., and Heitman, J. (2003). Phospholipid-binding protein Cts1 controls septation and functions coordinately with calcineurin in Cryptococcus neoformans. Eukaryot. Cell *2*, 1025–1035.

Fujita, M., Sugiura, R., Lu, Y., Xu, L., Xia, Y., Shuntoh, H., and Kuno, T. (2002). Genetic interaction between calcineurin and type 2 myosin and their involvement in the regulation of cytokinesis and chloride ion homeostasis in fission yeast. Genetics *161*, 971–981.

Ge, W., and Balasubramanian, M.K. (2008). Pxl1p, a paxillin-related protein, stabilizes the actomyosin ring during cytokinesis in fission yeast. Mol. Biol. Cell *19*, 1680–1692.

Goldman, A., Roy, J., Bodenmiller, B., Wanka, S., Landry, C.R., Aebersold, R., and Cyert, M.S. (2014). The calcineurin signaling network evolves via conserved kinase-phosphatase modules that transcend substrate identity. Mol. Cell *55*, 422–435.

Graef, I.A., Chen, F., and Crabtree, G.R. (2001). NFAT signaling in vertebrate development. Curr. Opin. Genet. Dev. *11*, 505–512.

Hameed, S., Dhamgaye, S., Singh, A., Goswami, S.K., and Prasad, R. (2011). Calcineurin signaling and membrane lipid homeostasis regulates iron mediated multidrug resistance mechanisms in Candida albicans. PLoS ONE *6*, e18684.

Hashimoto, Y., King, M.M., and Soderling, T.R. (1988). Regulatory interactions of calmodulin-binding proteins: phosphorylation of calcineurin by autophosphorylated Ca2+/calmodulin-dependent protein kinase II. Proc. Natl. Acad. Sci. USA *85*, 7001–7005.

Hirayama, S., Sugiura, R., Lu, Y., Maeda, T., Kawagishi, K., Yokoyama, M., Tohda, H., Giga-Hama, Y., Shuntoh, H., and Kuno, T. (2003). Zinc finger protein Prz1 regulates Ca2+ but not Cl- homeostasis in fission yeast. Identification of distinct branches of calcineurin signaling pathway in fission yeast. J. Biol. Chem. *278*, 18078–18084.

Ito, H., Fukuda, Y., Murata, K., and Kimura, A. (1983). Transformation of intact yeast cells treated with alkali cations. J. Bacteriol. *153*, 163–168.

Juvvadi, P.R., and Steinbach, W.J. (2015). Calcineurin orchestrates hyphal growth, septation, drug resistance and pathogenesis of Aspergillus fumigatus: where do we go from here? Pathogens *4*, 883–893.

Juvvadi, P.R., Fortwendel, J.R., Rogg, L.E., Burns, K.A., Randell, S.H., and Steinbach, W.J. (2011). Localization and activity of the calcineurin catalytic and regulatory subunit complex at the septum is essential for hyphal elongation and proper septation in Aspergillus fumigatus. Mol. Microbiol. *82*, 1235–1259.

Juvvadi, P.R., Lamoth, F., and Steinbach, W.J. (2014). Calcineurin-mediated regulation of hyphal growth, septation, and virulence in Aspergillus fumigatus. Mycopathologia *178*, 341–348.

Juvvadi, P.R., Lee, S.C., Heitman, J., and Steinbach, W.J. (2017). Calcineurin in fungal virulence and drug resistance: Prospects for harnessing targeted inhibition of calcineurin for an antifungal therapeutic approach. Virulence *8*, 186–197.

Kume, K., Koyano, T., Kanai, M., Toda, T., and Hirata, D. (2011). Calcineurin ensures a link between the DNA replication checkpoint and microtubule-dependent polarized growth. Nat. Cell Biol. *13*, 234–242.

Li, H., Rao, A., and Hogan, P.G. (2011). Interaction of calcineurin with substrates and targeting proteins. Trends Cell Biol. *21*, 91–103.

Lu, Y., Sugiura, R., Yada, T., Cheng, H., Sio, S.O., Shuntoh, H., and Kuno, T. (2002). Calcineurin is implicated in the regulation of the septation initiation network in fission yeast. Genes Cells *7*, 1009–1019.

Ma, Y., Sugiura, R., Koike, A., Ebina, H., Sio, S.O., and Kuno, T. (2011). Transient receptor potential (TRP) and Cch1-Yam8 channels play key roles in the regulation of cytoplasmic Ca2+ in fission yeast. PLoS ONE *6*, e22421.

McDonald, N.A., Lind, A.L., Smith, S.E., Li, R., and Gould, K.L. (2017). Nanoscale architecture of the *Schizosaccharomyces pombe* contractile ring. eLife *6*, 6.

Minami, T. (2014). Calcineurin-NFAT activation and DSCR-1 auto-inhibitory loop: how is homoeostasis regulated? J. Biochem. *155*, 217–226.

Moreno, S., Klar, A., and Nurse, P. (1991). Molecular genetic analysis of fission yeast Schizosaccharomyces pombe. Methods Enzymol. *194*, 795–823.

Park, H.S., Chow, E.W., Fu, C., Soderblom, E.J., Moseley, M.A., Heitman, J., and Cardenas, M.E. (2016). Calcineurin Targets Involved in Stress Survival and Fungal Virulence. PLoS Pathog. *12*, e1005873.

Pérez, P., Cortés, J.C., Martín-García, R., and Ribas, J.C. (2016). Overview of fission yeast septation. Cell. Microbiol. *18*, 1201–1207.

Pinar, M., Coll, P.M., Rincón, S.A., and Pérez, P. (2008). *Schizosaccharomyces pombe* Pxl1 is a paxillin homologue that modulates Rho1 activity and participates in cytokinesis. Mol. Biol. Cell *19*, 1727–1738.

Ren, L., Willet, A.H., Roberts-Galbraith, R.H., McDonald, N.A., Feoktistova, A., Chen, J.S., Huang, H., Guillen, R., Boone, C., Sidhu, S.S., et al. (2015). The Cdc15 and Imp2 SH3 domains cooperatively scaffold a network of proteins that redundantly ensure efficient cell division in fission yeast. Mol. Biol. Cell *26*, 256–269.

Rincon, S.A., and Paoletti, A. (2016). Molecular control of fission yeast cytokinesis. Semin. Cell Dev. Biol. *53*, 28–38.

Roberts-Galbraith, R.H., Chen, J.S., Wang, J., and Gould, K.L. (2009). The SH3 domains of two PCH family members cooperate in assembly of the Schizosaccharomyces pombe contractile ring. J. Cell Biol. *184*, 113–127.

Roberts-Galbraith, R.H., Ohi, M.D., Ballif, B.A., Chen, J.S., McLeod, I., McDonald, W.H., Gygi, S.P., Yates, J.R., 3rd, and Gould, K.L. (2010). Dephosphorylation of F-BAR protein Cdc15 modulates its conformation and stimulates its scaffolding activity at the cell division site. Mol. Cell *39*, 86–99.

Roy, J., and Cyert, M.S. (2009). Cracking the phosphatase code: docking interactions determine substrate specificity. Sci. Signal. *2*, re9.

Rustici, G., Mata, J., Kivinen, K., Lió, P., Penkett, C.J., Burns, G., Hayles, J., Brazma, A., Nurse, P., and Bähler, J. (2004). Periodic gene expression program of the fission yeast cell cycle. Nat. Genet. *36*, 809–817.

Sambrook, J., and Russell, D.W. (2001). Molecular Cloning: A Laboratory Manual (Cold Spring Harbor, N.Y.: Cold Spring Harbor Laboratory Press).

Sio, S.O., Suehiro, T., Sugiura, R., Takeuchi, M., Mukai, H., and Kuno, T. (2005). The role of the regulatory subunit of fission yeast calcineurin for in vivo activity and its relevance to FK506 sensitivity. J. Biol. Chem. *280*, 12231–12238.

Soriani, F.M., Malavazi, I., da Silva Ferreira, M.E., Savoldi, M., Von Zeska Kress, M.R., de Souza Goldman, M.H., Loss, O., Bignell, E., and Goldman, G.H. (2008). Functional characterization of the Aspergillus fumigatus CRZ1 homologue, CrzA. Mol. Microbiol. *67*, 1274–1291.

Stathopoulos, A.M., and Cyert, M.S. (1997). Calcineurin acts through the CRZ1/TCN1-encoded transcription factor to regulate gene expression in yeast. Genes Dev. *11*, 3432–3444.

Steinbach, W.J., Cramer, R.A., Jr., Perfect, B.Z., Asfaw, Y.G., Sauer, T.C., Najvar, L.K., Kirkpatrick, W.R., Patterson, T.F., Benjamin, D.K., Jr., Heitman, J., and Perfect, J.R. (2006). Calcineurin controls growth, morphology, and pathogenicity in Aspergillus fumigatus. Eukaryot. Cell *5*, 1091–1103.

Sugiura, R., Toda, T., Shuntoh, H., Yanagida, M., and Kuno, T. (1998). pmp1+, a suppressor of calcineurin deficiency, encodes a novel MAP kinase phosphatase in fission yeast. EMBO J. *17*, 140–148.

Sugiura, R., Sio, S.O., Shuntoh, H., and Kuno, T. (2002). Calcineurin phosphatase in signal transduction: lessons from fission yeast. Genes Cells *7*, 619–627.

Viana, R.A., Pinar, M., Soto, T., Coll, P.M., Cansado, J., and Pérez, P. (2013). Negative functional interaction between cell integrity MAPK pathway and Rho1 GTPase in fission yeast. Genetics *195*, 421–432.

Wachtler, V., Huang, Y., Karagiannis, J., and Balasubramanian, M.K. (2006). Cell cycle-dependent roles for the FCH-domain protein Cdc15p in formation of the actomyosin ring in Schizosaccharomyces pombe. Mol. Biol. Cell *17*, 3254–3266.

Willet, A.H., McDonald, N.A., and Gould, K.L. (2015). Regulation of contractile ring formation and septation in Schizosaccharomyces pombe. Curr. Opin. Microbiol. *28*, 46–52.

Yada, T., Sugiura, R., Kita, A., Itoh, Y., Lu, Y., Hong, Y., Kinoshita, T., Shuntoh, H., and Kuno, T. (2001). Its8, a fission yeast homolog of Mcd4 and Pig-n, is involved in GPI anchor synthesis and shares an essential function with calcineurin in cytokinesis. J. Biol. Chem. *276*, 13579–13586.

Yoshida, T., Toda, T., and Yanagida, M. (1994). A calcineurin-like gene ppb1+ in fission yeast: mutant defects in cytokinesis, cell polarity, mating and spindle pole body positioning. J. Cell Sci. *107*, 1725–1735.

Zhang, Y., Sugiura, R., Lu, Y., Asami, M., Maeda, T., Itoh, T., Takenawa, T., Shuntoh, H., and Kuno, T. (2000). Phosphatidylinositol 4-phosphate 5-kinase Its3 and calcineurin Ppb1 coordinately regulate cytokinesis in fission yeast. J. Biol. Chem. *275*, 35600–35606.

STAR★METHODS

KEY RESOURCES TABLE

REAGENT or RESOURCE	SOURCE	IDENTIFIER
Antibodies		
rabbit anti-HA tag antibody-ChIP Grade	Abcam	Cat# ab9110, RRID:AB_307019
rabbit GFP tag polyclonal antibody	Invitrogen	Cat#A-6455;RRID AB_221570
rat anti-HA-peroxidase, high affinity (3F10)	Roche	Cat# 12013819001, RRID:AB_390917
Living colors A.v. monoclonal antibody (JL8)	Clontech	Cat#632380 RRID:AB_10013427
anti-GST-HRP conjugate	GE Healthcare	Cat#RPN1236, RRID:AB_771429
mouse anti-actin monoclonal (C4)	MP biomedicals	Cat# 08691001, RRID:AB_2335127
Chemicals, Peptides, and Recombinant Proteins		
Amylose resin	New England Biolabs	Cat#E8021S
Glutathione Sepharose 4B	GE Healthcare	Cat#17-0756-01
Protein A Sepharose CL-4B	GE Healthcare	Cat#17-0780-01
Protease/Phosphatase inhibitor cocktail (100X)	Cell Signaling	Cat#5872S
Phos-tag acrylamide AAL-107	Wako	Cat#304-93521
Lectin from Glycine max (soybean)	Sigma	Cat#L-1395-5mg
Lambda protein phosphatase	New England Biolabs	Cat#P0753S
CN (human) recombinant	Enzo	Cat#BML-SE163-5000
Calmodulin (human) recombinant	Enzo	Cat#BML-SE329-0001
CN assay buffer (2X)	Enzo	Cat#BML-KI128-0020
Deposited Data		
Raw Data	This study	Mendeley Data; https://doi.org/10.17632/bp87npk532.1
Experimental Models: Organisms/Strains		
Fission yeast strains used in this study are detailed in Table S1	N/A	N/A
Oligonucleotides		
Generation of Pxl1-M3 mutation; Fw primer:5′ CGCGGATCC ATATGCATTCACCAATTCCAGAAT3′	Biomers	N/A
Generation of Pxl1-M3 mutation; Rv primer:5′ CTACGAT TGGAAAGTTTACTGGATTTCgcagcAGcAgcAGcAGc AAGTTGTTTGGATGCGAAGGTTTTTTGTCTG 3′	Biomers	N/A
Generation of Pxl1-M4 mutation; Fw primer: 5′ GCAA GAAATGCCGTAAAgCCgcTgcGGcGgcCgc TGTAAAAGGGTCTGATGGTGAATATCATAG 3′	Biomers	N/A
Generation of Pxl1-M4 mutation; Rv primer: 5′ CGCGGA TCCTTAATCCAAATTAAACTTGACTGA 3′	Biomers	N/A
Generation of N-Pxl1-Ppb1 chimera; Fw primer: 5′ TATATGCT AGCATGACTTCGGGTCCTCATAATT 3′	Sigma-Aldrich	N/A
Generation of N-Pxl1-Ppb1 chimera; Rv primer: 5′ ATATAGG ATCCTACAAAGAGCTTTTCTTATCTG 3′	Sigma-Aldrich	N/A
Creation of MBP-PPb1-HA; Fw primer: 5′ ATATAT TCT AGA ATGACTTCGGGTCCTCATAATTTAG 3′	Sigma-Aldrich	N/A
Creation of MBP-PPb1-HA; Rv primer: 5′ ATATAT TCT AGA TCAGCACTGAGCAGCGTAATC 3′	Sigma-Aldrich	N/A
Recombinant DNA		
pJK148-GFP-Pxl1-M3	This study	N/A
pJK148-GFP-Pxl1-M4	This study	N/A
pJK148-GFP-N-Pxl1-Ppb1	This study	N/A

(*Continued on next page*)

Continued

REAGENT or RESOURCE	SOURCE	IDENTIFIER
pJK148-N-Pxl1-Ppb1	This study	N/A
pJC20-GST-Pxl1	This study	N/A
pJC20-GST-Pxl1-M3	This study	N/A
pJC20-GST-Pxl1-M4	This study	N/A
pMAL-p2-Ppb1-HA	This study	N/A
Software and Algorithms		
ImageJ	NIH	https://imagej.nih.gov/ij/
SoftWorx software 6.0	GE Healthcare	N/A
Graphpad Prism	Graphpad Software	https://www.graphpad.com
Other		
μ-slide 8 well uncoated	Ibidi	Cat#80821

CONTACT FOR REAGENT AND RESOURCE SHARING

Further information and requests for resources and reagents should be directed to the Lead Contact, Pilar Pérez (piper@usal.es).

EXPERIMENTAL MODEL AND SUBJECT DETAILS

Fission yeast growth conditions

All the *Schizosaccharomyces pombe* strains used in this study were isogenic to 972 h- and 975 h+, and are enumerated in Table S1. Standard *S. pombe* media and genetic manipulations were used (Moreno et al., 1991). Basically, cells were grown either in rich medium (YES) or in minimal medium (EMM) with appropriate supplements at 25, 28 or 36°C depending on the type of experiment, as indicated in the figure legends. EMM+S (1.3M sorbitol) was used with P*nmt81-bgs1*$^+$ and derived strains. For repression experiments in strains carrying the P*nmt81* promoter, early log-phase cells incubated in EMM+S were diluted with the same medium plus 20 μg/ml thiamine (+T). Cell growth was monitored by measuring the OD_{600} of early-log phase cell cultures. SPA medium was used for genetic crosses and mutant strains were selected by tetrad dissection, random spore dissection or random spore analysis.

METHOD DETAILS

Recombinant DNA methods

All DNA manipulations were carried out by established methods (Sambrook and Russell, 2001). Plasmid DNA was introduced into *S. pombe* cells by an improved lithium acetate method (Ito et al., 1983).

The Pxl1 mutated proteins were generated by PCR site-directed mutagenesis using the appropriate primers and a KS Bluescript plasmid containing the *pxl1*$^+$ ORF as template (lab stock plasmid described in Pinar et al., 2008). All the mutations to generate amino acid changes were confirmed by DNA sequencing and clones as *NdeI*/*BamHI* fragment into the fission yeast integrative vector pJK148 or into the pJC20 vector for expression in *E.coli.* GST epitope was 5′inserted as *NdeI*/*NdeI* into pJC20 carrying the different ORFs.

GFP-N-Pxl1-Ppb1 chimera was constructed by amplifying the *ppb1*$^+$ ORF with the appropriate primers, which was then ligated as *NheI-BamHI* into a KS Bluescript plasmid containing the *GFP* ORF fused to the *pxl1*$^+$ N-terminal fragment (771 base pairs) and the 5′ and 3′ non coding flanking regions of *pxl1*$^+$ (lab stock plasmid). Construction of the *N-Pxl1-Ppb1* without the GFP was generated from the KS-*GFP-Pxl1-Ppb1* plasmid previously described, digesting with *NdeI* to split the *GFP* coding region and re-ligating the remaining plasmid. The resulting constructs were then cloned into pJK148 as PstI/*SacII* for *S. pombe* chromosome integration at the *leu1*$^+$ locus.

The Maltose Binding Protein (MBP)-Ppb1-HA was generated amplifying by PCR with the appropriate primers, the *ppb1-HA* fragment from a strain in which *ppb1*$^+$ was endogenously tagged in C terminus with the HA epitope. The fragment amplified was then cloned into the *XbaI* site of the pMAL-p2 vector.

General protein methods

Whole cell extracts were prepared in lysis buffer (20 mM Tris-HCl, pH 8.0, 2 mM EDTA, 100 mM NaCl, and 0.5% NP-40, containing 100mM p-aminophenyl methanesulfonyl fluoride, 2g/ml leupeptin, and 2g/ml aprotinin). Cell extracts (1mg) were then incubated with anti-HA polyclonal antibody (ab9110, Abcam) or anti-GFP polyclonal serum (A6455, Invitrogen) and protein A-Sepharose beads for 2-4h at 4°C. The beads were washed four times with lysis buffer and then they were resuspended in sample buffer. The immunoprecipitates were then analyzed by western blot.

Protein extracts for analysis of phosporylation status were obtained by TCA precipitation.

Recombinant protein production in *E. coli*

E.coli BL-21 strain was used for the expression of recombinant proteins. Bacterial induction was done by the addition of 0.4 mM IPTG during 4h at 28°C. Then, the cells were collected and lysed by sonication (14 μm amplitude for 1 min, 3 repeats) in PBS containing protease inhibitors and 0.4 mg/ml lysozime. Then 1% Triton X-100 was added and the cells were centrifuged. The supernatant was collected and incubated with glutathione-Sepharose beads (50% in PBS) during 2h at 4°C. Afterward, glutathione-Sepharose beads with GST-Pxl1 bound, were washed 4 times with PBS and resuspended in buffer (50 mM Tris-ClH pH 7.5, 20 mM NaCl, 0.5% NP-40, 10% Glycerol; 0,1mM DTT, 1mM NaF, and 2mM $MgCl_2$ containing 100 μM p-aminophenylmethanesulphonyl fluoride, leupeptin, and aprotinin) before its used in pull-down assays. The amount of purified GST-Pxl1 was quantified by Coomassie Blue staining of SDS-PAGE gels, and compared to Bovine Serum Albumin (BSA) standards of known concentration.

Recombinant MBP-Ppb1-HA was produced from the pMAL-p2 vector for periplasmic expression, purified by affinity chromatography with amylose resin (New England Biolabs) and eluted with maltose.

Pull down of Ppb1-HA or Cnb1-HA with GST-Pxl1

Cell extracts from wild-type, *cnb1*Δ or *ppb1*Δ cells expressing *ppb1-HA* or *cnb1-HA* from their own promoter, were obtained by mechanical breakage of the cells using glass beads and a FastPrep. Cells were resuspended in 500 μL of lysis buffer (50 mM Tris-ClH pH 7.5, 20 mM NaCl, 0.5% NP-40, 10% Glycerol; 0,1mM DTT, 1mM NaF, and 2mM $MgCl_2$ containing 100 μM p-aminophenylmethanesulphonyl fluoride, leupeptin, and aprotinin). 10 μg of GST-Pxl1 or GST-Pxl1 fragments previously obtained from *E. coli* expression, purified and coupled to gluthatione-Sepharose beads, were used to precipitate Ppb1-HA or Cnb1-HA from 2 mg of the total cell lysates. The extracts were incubated with the beads for 2 h at 4°C, washed four times, and the bound proteins were released. The proteins were analyzed by SDS-PAGE and blotted against anti-HA high affinity monoclonal antibody (Clone 3F10, Roche Molecular Biochemicals) to detect the corresponding HA-tagged protein. The total amount of HA-tagged proteins from the extracts were determined by western blot and using the same anti-HA monoclonal antibody.

For the pull-down of recombinant MBP-Ppb1-HA with GST-Pxl1 equal quantities of recombinant MBP-Ppb1-HA and GST-Pxl1 were mixed in binding buffer (200 mM Tris-HCl pH 8, 137 mM NaCl, 0.1% NP-40, 10% Glycerol, 2mM EDTA) and incubated with Glutation-Sepharose beads (50% in the same buffer) during 2h at 4°C.

The amount of MBP-PPb1-HA bound to GST-Pxl1 was determined by western blot using anti-HA monoclonal antibody.

Western-Blot of synchronized cell cultures

Cdc25-22 cells containing Cdc15-HA or GFP-Cdc15, treated or untreated with FK506 (5μg/ml) were grown to mid log phase, shifted to 36°C for 4 h and then released to permissive temperature of 25°C. Samples were collected every 30 min and processed for western blot analysis. Protein extracts from the different time-points were obtained as above and prepared by TCA precipitation. In addition, another sample of cells for each time-point was collected and fixed with cold 70% ethanol for subsequent DAPI and calcofluor staining to monitor cell cycle progression and septation.

In vitro CN phosphatase assay

Cell extracts from *cdc25-22 GFP-cdc15* synchronized cultures (in anaphase, 60 minutes after culture release) and treated with FK506 (5μg/ml, 4h) were obtained in lysis buffer (20mM Tris-HCl, 130mM NaCl, 0.5% NP40) supplemented with proteases and phosphatases inhibitors cocktail (Cell Signaling) and PMSF. The GFP-Cdc15 protein was immunopurified from the supernatant by incubation with anti-GFP polyclonal antibody (Molecular Probes. Invitrogen) and protein-A Sepharose beads (GE Healthcare). The immunoprecipitates were collected by centrifugation and washed three times with lysis buffer without proteases and phosphatases inhibitors cocktail. Then GFP-Cdc15 bound to beads was incubated with KI-128 assay buffer (50mM Tris-HCl, 100mM NaCl, 6mM $MgCl_2$, 0.5 mM DTT, 0.025% NP-40 and 0.25mM $CaCl_2$) plus 1μg of human recombinant Calmodulin (Enzo) and 500 units of human recombinant CN (Enzo) for 1 hour at 30°C. For lambda phosphatase assay, used as a control, the immunoprecipitated GFP-Cdc15 bound to beads was incubated with PMP buffer (50 mM HEPES pH 7.5, 100 mM NaCl, 2 mM DTT, 0.01% Brij 35, 1 mM $MnCl_2$) and 400 units of lambda phosphatase (New England Biolabs) for 1 hour at 30°C. After the incubation with the CN or lambda phosphatases or with CN buffer alone, the supernatant was removed and the beads with GFP-Cdc15 bound were resuspended in Laemmli sample buffer, boiled and centrifuged. Finally, GFP-Cdc15 was detected by western blot using anti-GFP monoclonal antibody (JL-8, Clontech).

Microscopy techniques and data analysis

For calcofluor staining, a solution of Calcofluor White (50 μg/ml final concentration) was directly added to early logarithmic phase cells.

Fluorescence images obtained with a Personal DeltaVision System (GE Healthcare) were corrected by 3-D deconvolution (conservative ratio, 10 iterations, and medium noise filtering) using the SoftWoRx imaging software (6.0, GE Healthcare).

For maximal projection of the cell and three-dimensional reconstructions of the cell middle region in Figure 1G, images were obtained in Z stacks of 22 slices at 0.25 μm intervals to ensure that the complete cell is covered and the obtained images were processed with the 3D projection function of the ImageJ software.

For time-lapse imaging, 0.3 mL of early log-phase cell cultures were placed in a well from a μ-Slide 8 well (Ibidi) previously coated with 10 μl of 1 mg/ml soybean lectin (Sigma-Aldrich). Cells were left for 1 min to attach to the well bottom and culture media was removed carefully. Then, cells were washed three times with the same media and finally 0.3 mL of fresh media were added (Cortés et al., 2012). Experiments were performed at 25°C or 28°C and single middle planes were taken at the time points stated in each figure. Time-lapse images were acquired using a spinning disk confocal microscope (Olympus IX81 with Roper technology) with a 100X/1.40 Plan Apo lens and controlled by Metamorph 7.7 software.

Line scans in Figures 1 and 3 were made by drawing a line along all the septum length, and measuring the intensities of pixels of the red and green fluorescence through the plot profile function of the ImageJ software. The positions of the offset septa in Figure 1F were calculated from calcofluor-stained images with the ImageJ software by measuring the distance from the septum to the closest tip, subtracting this value from the value corresponding to half of the cell length, and calculating the percentage of the resulting value respect to the total cell length.

Total fluorescence analysis of a single focal plane of GFP-Ppb1 and GFP-Pxl1 in Figures 4C and Figure 6 respectively, was quantified with ImageJ software by selecting the middle region of each cell containing the ring. Next the background fluorescence of each cell was subtracted (ImageJ). After quantification of the GFP-Pxl1 fluorescence, the length of the corresponding septum was measured by drawing a line through the septum in the calcofluor-staining micrograph. Scatter dot plots were represented using GraphPad Prism software.

QUANTIFICATION AND STATISTICAL ANALYSIS

No statistical methods were used to predetermine sample size. Bar graphs shown in Figures 1E, 1F, 1G, 2B, 4B and 5C represent the percentage of cells displaying the indicated phenotypes. Error bars represent the standard deviation of the data. The n value and the number of technical replicates are indicated in the corresponding figure legends. In the scatterplots in Figures 4C and 6B and S3 the black lines represent the mean and SEM. Statistical analysis were done using Graphpad Prism software using the tests specified in the figure legends. Comparisons of two conditions were tested by unpaired t test. Multiple comparisons were tested by two-way ANOVA with post-test (Tukey's and Bonferroni's). Statistical significances were marked by ****$p < 0.0001$.